Numerical simulations for the bearing capacity of circular footings

Mikaël Kalfa, Abdul-Hamid Soubra, Dalia S. Youssef Abdel Massih

NUMERICAL SIMULATIONS FOR THE BEARING CAPACITY OF CIRCULAR FOOTINGS

M. KALFA and A.-H. SOUBRA
University of Nantes, GeM, UMR CNRS 6183, Bd. de l'université,
BP 152, 44603 Saint-Nazaire cedex, France
Abed.Soubra@univ-nantes.fr

D. S. YOUSSEF ABDEL MASSIH
CNRS Lebanon, Bhanes, Lebanon
Dalia@cnrs.edu.lb

SUMMARY: The aim of this paper is the computation of the failure loads of a rough rigid circular footing subjected to a vertical or inclined loading using the finite difference code *FLAC*^{3D}. For the case of vertical load, controlled downward vertical velocities are applied to the footing nodes until a steady state of plastic flow is obtained in the soil. For the construction of the (H,V) failure envelope of an inclined load, a uniform normal stress distribution is first applied to the base of the footing and the system is solved until it reaches an equilibrium state. Then, controlled horizontal velocities are applied to the nodes of the footing bottom until a steady state of plastic flow is obtained in the soil. Results of failure loads are presented and compared with those of other authors. Finally, the normal and shear contact stresses acting at the soil-footing interface are presented and discussed.
Keywords: bearing capacity, circular footing, limit loads, numerical simulations.

INTRODUCTION

The ultimate bearing capacity of a strip footing subjected to a central vertical load has long been a topic for research. However, when the footing is circular and subjected to an inclined and/or an eccentric load, the scientific research concerning this issue has essentially occurred during the last few decades. Traditionally, geotechnical engineers make use of empirical reduction coefficients provided by the different codes. In this paper, numerical simulations of the failure loads of a rough rigid circular footing subjected to a vertical or inclined loading are performed using the Lagrangian explicit

NUMERICAL SIMULATIONS

This section focuses on the numerical modeling of the failure loads of a rough rigid circular footing, of diameter $D = 2\,m$, resting on a (c, φ) soil and subjected to a vertical or an inclined load using $FLAC^{3D}$.

$FLAC^{3D}$ (Fast Lagrangian Analysis of Continua) is a commercially available three-dimensional finite difference code in which an explicit Lagrangian calculation scheme and a mixed discretization zoning technique are used. It includes an internal programming option (FISH) which enables the user to add his own subroutines. Although a static (*i.e.* non-dynamic) mechanical analysis is required, the equations of motion are used in this code. The solution to a static problem is obtained through the damping of the dynamic process by including terms that gradually remove kinetic energy from the system. In $FLAC^{3D}$, the application of velocities or stresses on a system creates unbalanced forces. Damping is introduced in order to remove these forces or to reduce them to very small values compared to the initial ones. Stresses and deformations are calculated at several small timesteps (called hereafter cycles) until a steady state of static equilibrium or plastic flow is achieved. The convergence to this state can be controlled by a maximal prescribed value of the unbalanced forces for all elements of the model.

For the computation of the limit loads of a rough rigid circular footing, the following procedure is adopted (when applicable) before any simulation: geostatic stresses are first applied to the soil, then several cycles are run in order to attain a steady state of static equilibrium and finally, the obtained displacements are set to zero in order to obtain the footing displacement due only to the footing loads.

Vertical load

Because of symmetry, only one quarter of the entire soil domain of diameter $7D$ and depth $2.5D$ is considered. The bottom and the outer vertical boundary of the soil domain are far enough from the footing and thus do not disturb the soil mass in motion (*i.e.* velocity field) for all the soil configurations studied in this paper. A non uniform mesh composed of 2420 zones is used (Figure 1). The soil region under the footing was divided horizontally into four equal angular sectors of 22.5° each and 10 rings whose size gradually decreases from the center to the periphery of the footing where very high stress gradients are developed. Beyond the footing, the soil domain was divided horizontally into four equal angular sectors of 22.5° each and into 20 rings whose size increases gradually from the foundation periphery to the outer vertical cylindrical boundary. Vertically, the soil domain was divided into 20 zones whose size decreases gradually from the bottom of the domain to the ground surface. Concerning the footing, it is subdivided horizontally into four equal angular sectors and five equal rings and vertically into one single zone. The nodes of the interface are those of the soil. Each quadrilateral element of the interface is automatically divided by $FLAC^{3D}$ into two triangular elements.

For the displacement boundary conditions of the vertical load case (Figure 1), the bottom boundary was assumed to be fixed and the outer vertical cylindrical boundary was constrained in motion in the horizontal X and Y directions. Concerning the two symmetrical vertical planes, they were constrained in motion in the direction perpendicular to these planes.

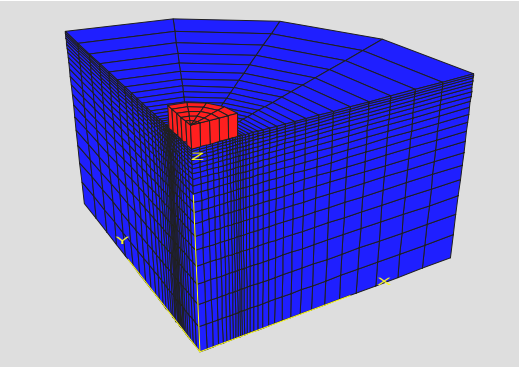

Fig 1: *Soil domain and mesh used in FLAC^{3D}*

A conventional elastic-perfectly plastic model based on the Mohr-Coulomb failure criterion is used to represent the soil. The soil elastic properties used are the shear modulus $G = 100\,\text{MPa}$ and the bulk modulus $K = 200\,\text{MPa}$ (for which the equivalent Young's modulus and Poisson's ratio are respectively $E = 257\,\text{MPa}$ and $\nu = 0.3$). The values of the soil shear strength parameters used will be given later. The circular footing of diameter $2\ \text{m}$ and depth $0.5\ \text{m}$ is modeled by a weightless material that follows an elastic model. The footing elastic properties used are the Young's modulus $E = 25\ \text{GPa}$ and the Poisson's ratio $\nu = 0.4$. Compared to the soil elastic properties, these values are well in excess of those of the soil and ensure a rigid behavior of the footing. Notice that the soil and footing elastic properties have a negligible effect on the failure load.

The footing is connected to the soil via interface elements that follow Coulomb law. The interface is assumed to have a friction angle equal to the soil angle of internal friction and the same dilation angle and cohesion as the soil in order to simulate a perfectly rough soil-footing interface. Normal stiffness $K_n = 1\,G\text{Pa/m}$ and shear stiffness $K_s = 1\,G\text{Pa/m}$ are assigned to this interface. These parameters do not have a major influence on the failure load.

For the simulation of the ultimate vertical load, a displacement-controlled method is used. In this method, an optimal downward vertical velocity (*i.e.* displacement per timestep) is applied to the nodes of the footing. Damping of the system is performed by running several cycles until a steady state of plastic flow develops in the soil beneath the footing. This state is achieved when both conditions (i) a constant footing load and (ii) small values of the unbalanced forces, are satisfied as the number of cycles increases. The number of cycles required to reach this state depends on the value of the applied velocity. At each cycle, the vertical footing load is obtained by using a *FISH* function that calculates the integral of the normal stress components for all elements in contact with the footing. The value of the vertical footing load at the plastic steady state is the ultimate footing load. The ultimate bearing capacity is then obtained by dividing this load by the footing area. An optimal velocity must be chosen in order to reach a value of the ultimate bearing capacity close to the smallest most critical one (corresponding to a very small velocity) with a reasonable computation time. Several tests were done. It was found that when cohesion is present in the soil, a velocity of 10^{-7} m/timestep is adequate since it gives a solution close to the one obtained with a smaller velocity of 10^{-8}. However, for a cohesionless soil, a velocity of 10^{-8} m/timestep was necessary especially for values of the angle of internal friction of the soil smaller than 30°. For $\varphi \succ 30°$, a velocity of 10^{-7} m/timestep led to acceptable results in comparison to the 10^{-8} m/timestep velocity.

Inclined load

Because of the absence of loading symmetry, only one half of the entire soil domain of diameter $7D$ and depth $2.5D$ is considered in this section. The computation of a given point of the (H,V) failure envelope (where H and V are respectively the horizontal and vertical ultimate footing loads) can be summarized as follows: firstly, a central vertical load (smaller than the vertical ultimate one) is applied to the footing *via* uniform nodal stresses S_{zz} acting at the nodes situated at the base of the footing. Then, damping of the system is introduced by running several cycles until a steady state of static equilibrium develops in the soil underneath the footing. This state is achieved when very small values of the unbalanced forces are obtained as the number of cycles increases. Secondly, a controlled horizontal velocity (*i.e.* displacement per timestep) is applied, in the X direction, to the nodes situated at the bottom of the footing. Again, damping of the system is performed by running several cycles until a steady state of plastic flow develops in the soil beneath the footing. This state is achieved when both conditions (i) a constant horizontal footing load along the interface and (ii) small values of unbalanced forces in the soil mass, are obtained as the number of cycles increases. The horizontal footing load is obtained at each cycle by using a *FISH* function that calculates the integral of the shear stress components for all elements in contact with the footing. The value of the horizontal load at the plastic steady state is the ultimate horizontal load that led to soil failure. The corresponding horizontal footing stress is obtained by dividing this load by the footing area. The ultimate bearing capacity is obtained by dividing the vertical applied load by the footing area.

NUMERICAL RESULTS

For each type of soil, several runs are done in the aim to perform numerical calculations with the optimal velocity. Computations are carried out for an associative flow rule, as it is often (implicitly) assumed in most methods in bearing capacity, in order to enable a fair comparison with other authors' results. Thus, a dilation angle equal to the angle of internal friction was used.

Vertical load

Figure 2 presents the bearing capacity factors obtained from FLAC3D and those given by other authors. For N_γ, there is a good agreement between the present values and those given by Kumar and Ghosh 1 using the slip line method. The solutions presented by Bolton and Lau 2 are greater than the present solutions. The difference is greater than 40%. However, the results given by Salençon and Matar 3, Erickson and Drescher 4, Cassidy and Houlsby 5 and Martin 6 are smaller than the present solutions. The difference is about 35%. For N_c, there is a good agreement between the present values and those given by Manoharan and Dasgupta 7, Erickson and Drescher 4 and Martin 6. However, Bolton and Lau2 largely underestimate the bearing capacity factor N_c. Finally, it should be mentioned that the Eurocode 7 highly underestimate both bearing capacity factors N_γ and N_c. Thus, it gives conservative results.

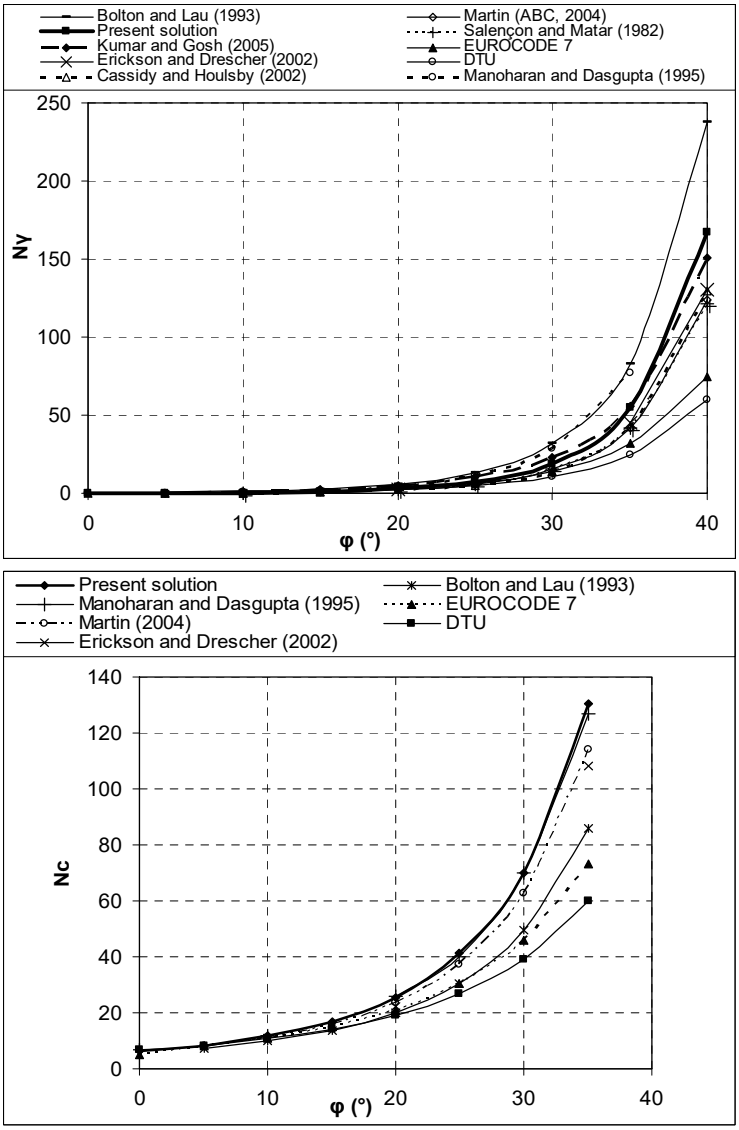

Fig. 2: *Comparison of present N_γ and N_c factors with those of other authors.*

Inclined load

Figures 3, 4 and 5 show the failure envelopes obtained from the numerical *FLAC*^{3D} simulations for the three cases considered, *i.e.* (i) a purely cohesive soil with $c_u = 50\,\text{kPa}$, (ii) a weightless frictional cohesive soil with $c = 20\,\text{kPa}$ and $\varphi = \psi = 30°$ and, (iii) a cohesionless ponderable soil with $\varphi = \psi = 30°$ and $\gamma = 18\,\text{kN/m}^3$. Notice that in these diagrams, the simulation method presented for the vertical load case was used for the point corresponding to $H = 0\,\text{kN}$. For the remaining points of these diagrams, the method presented for the inclined load was used.

In the case of a purely cohesive soil (Figure 3), one can easily see that a sliding along the soil-footing interface may occur for small values of the vertical load. The corresponding horizontal stress at the soil-footing interface was found equal to c_u. For a weightless frictional and cohesive soil, the codes of practice largely underestimate the bearing capacity for small load inclinations (Figure 4). However, for great load inclinations, the French code of practice DTU overestimates the bearing capacity. For a cohesionless soil (Figure 5), the codes of practice always underestimate the limit loads of the foundation.

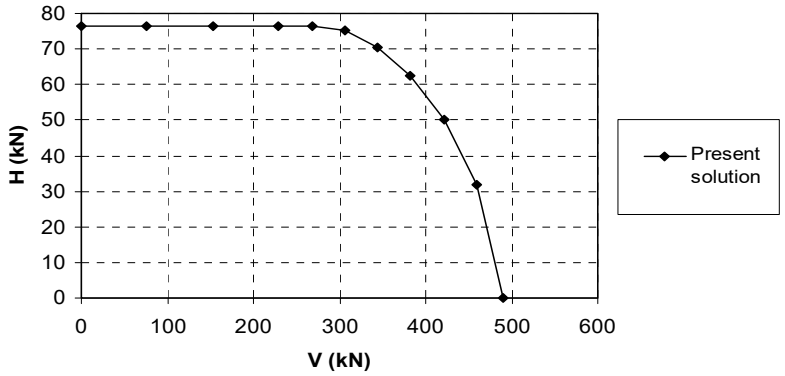

Fig. 3: *Failure envelope of a purely cohesive soil* ($\varphi_u = 0°$ and $c_u = 50kPa$).

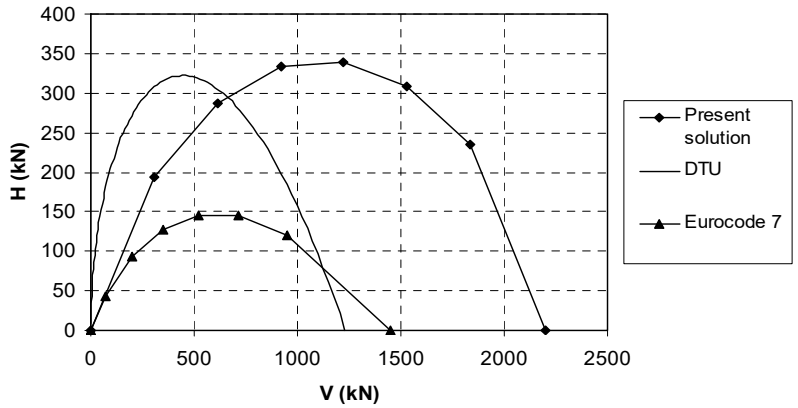

Fig. 4: *Failure envelope of a weightless frictional cohesive soil* ($\varphi = 30°$ and $c = 20kPa$)

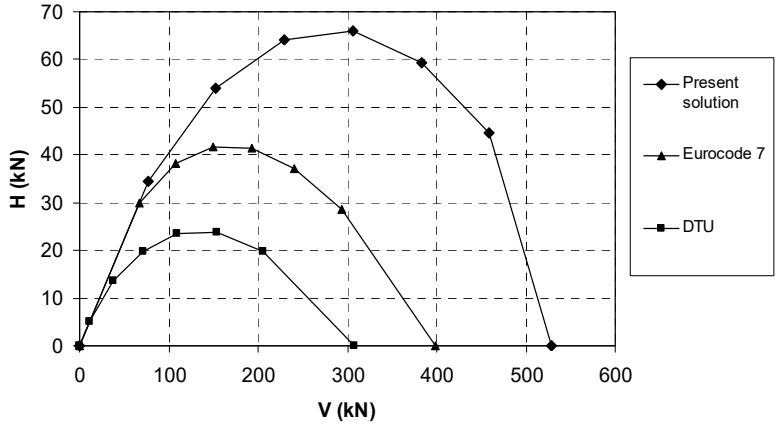

Fig. 5: *Failure envelope of a cohesionless soil* ($\varphi = 30°$ and $\gamma = 18kN/m^3$).

Contrary to the vertical load case where the normal and shear stress distributions along the different diameters of the foundation are identical, there is a progressive evolution of these stresses from a diameter to the next one in the present case. Figures 6–11 present the distributions of the normal (σ) and shear (τ) stresses for the three configurations studied in this paper. For each configuration, one can observe the distribution of these stresses for different values of S_{zz}, (*i.e.* for different load inclinations) and along two different positions of the diameter (in the direction of loading 'Section X-X' and in the orthogonal direction to the loading 'Section Y-Y').

For the clay, as well as the weightless frictional and cohesive soil, except at the footing edges which are singular points, a quasi-uniform normal stress distribution was observed (Figures 6 and 8). For the shear stress distribution, both positive and negative shear stresses were observed in the direction of loading ('sections X-X') for large vertical loads (Figures 7 and 9). However, for small vertical loads, shear stresses become all negative in order to counter weight the horizontal external load. At the limit, for smaller values of the vertical load, shear stresses tend to be constant. This state corresponds to a sliding along the soil-footing interface.

For the sand, a quasi-uniform normal stress distribution was observed near the footing center (Figure 10). It tends to zero at the edges of the footing. Concerning the shear stress distribution, both positive and negative shear stresses were observed for large vertical loads (Figure 11). However, for small vertical loads corresponding to large horizontal loads, shear stresses become essentially negative in order to counter weight the horizontal external load. As for the normal stress distribution, the shear stress tends to zero at the footing edges.

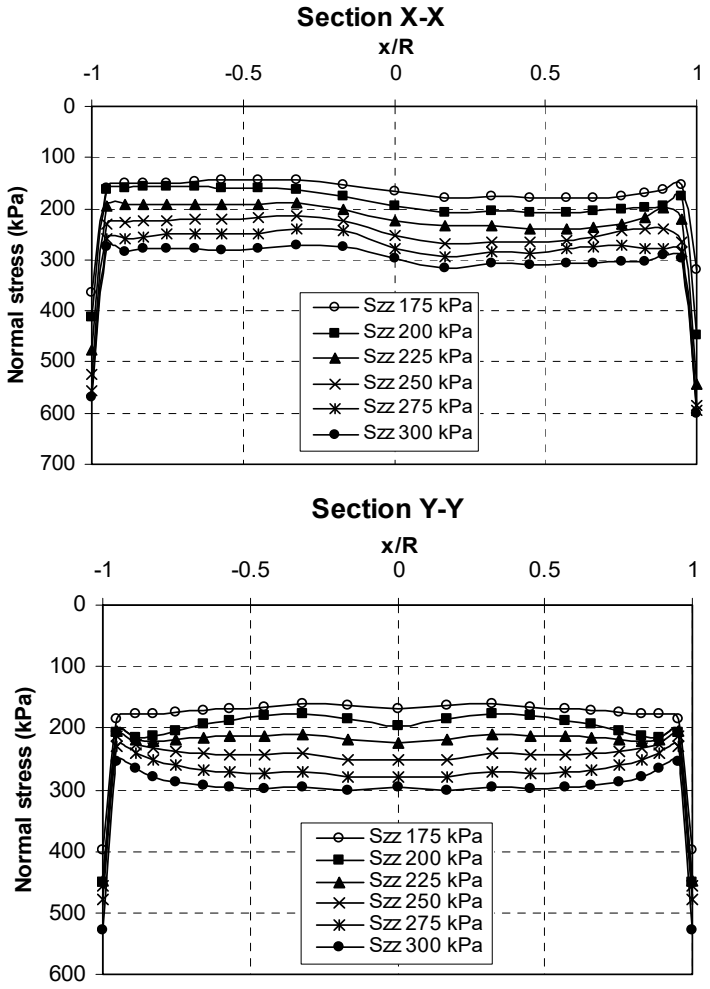

Fig. 6: *Normal* (σ) *stress distribution along X-X and Y-Y. Purely cohesive soil.*

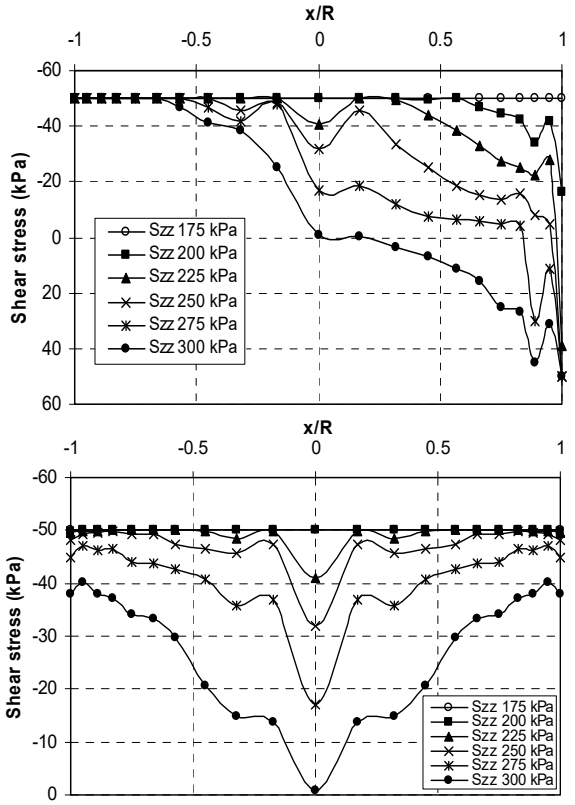

Fig. 7: *Shear* (τ) *stress distribution along X-X (upper) and Y-Y (lower) – Purely cohesive soil.*

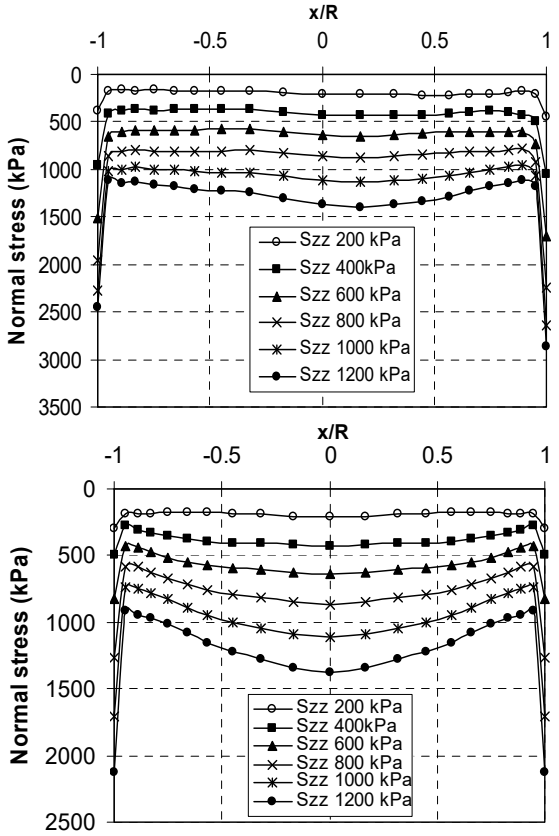

Fig. 8: *Normal* (σ) *stress distribution along X-X (upper) and Y-Y (lower) – Weightless frictional and cohesive soil.*

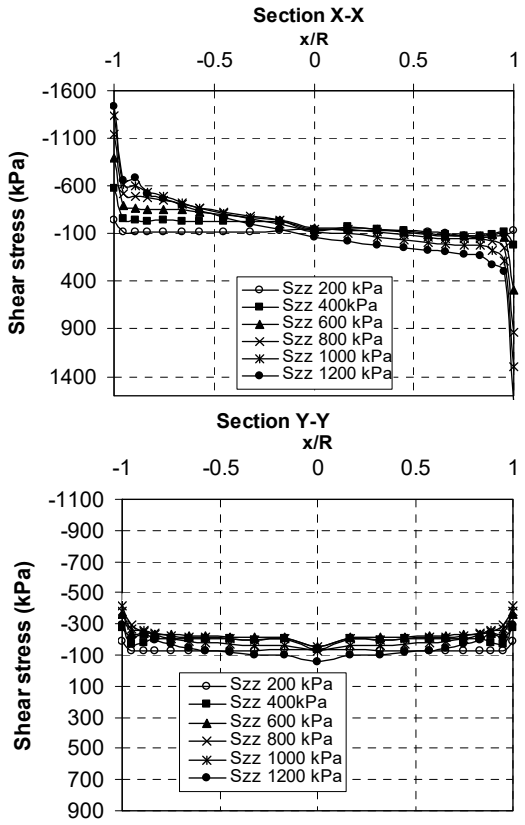

Fig. 9: *Shear* (τ) *stress distribution along X-X (upper) and Y-Y (lower) – Weightless frictional and cohesive soil.*

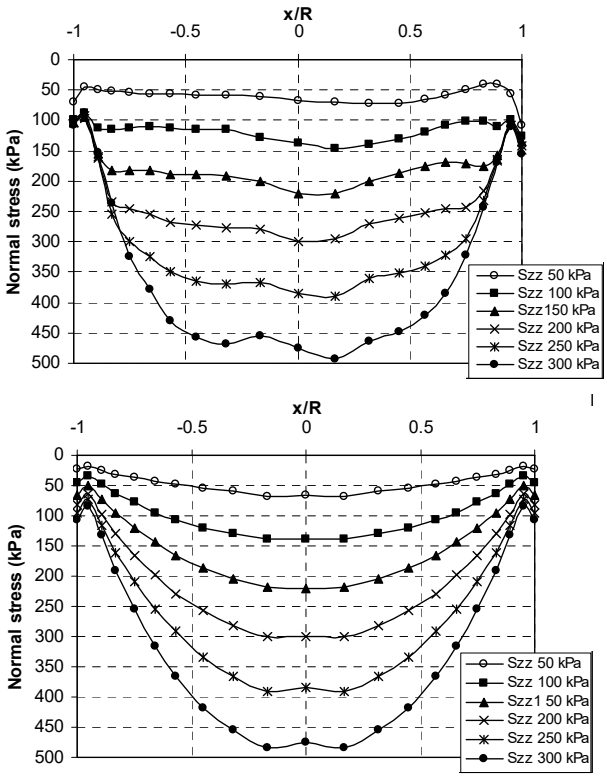

Fig. 10: *Normal* (σ) *stress distribution along X-X (upper) and Y-Y (lower) – Cohesionless soil.*

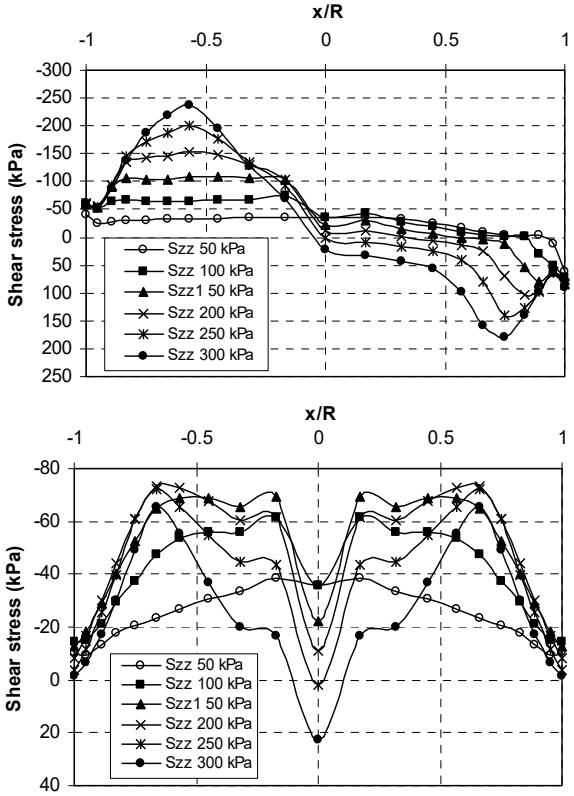

Fig. 11: *Shear* (τ) *stress distribution along X-X (upper) and Y-Y (lower) – Cohesionless soil.*

The distribution of the mobilized friction angle δ at the soil footing interface is presented in Figure 12 for the X-X section in the case of sand. The value of δ is given by:

$$\delta = \arctan\left(|\tau|/\sigma\right) \tag{1}$$

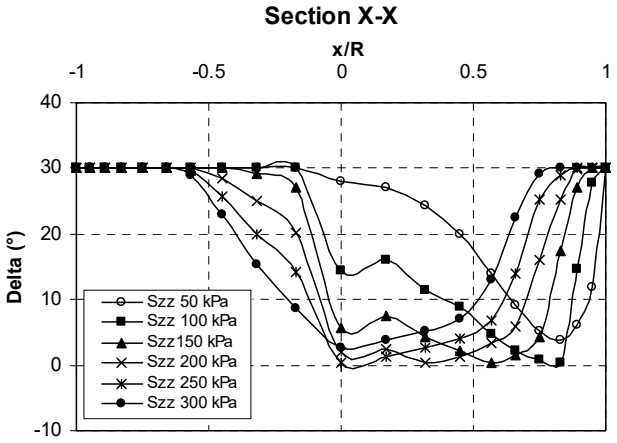

Fig. 12: *Mobilized friction angle* δ *at the soil footing interface – Cohesionless soil.*

A mobilized angle equal to the angle of internal friction (*i.e.* $\delta = \varphi = 30^\circ$) is observed along some distances of the interface near the edges of the footing. These distances are the ones for which sliding occurs.

CONCLUSIONS

Numerical *FLAC*^{3D} simulations were performed for the calculation of the ultimate bearing capacity of a circular footing subjected to a vertical or an inclined load. A displacement-controlled approach was used. It was shown that:

- For a vertical load, the N_γ values are in good agreement with those given by the slip line method by Kumar and Ghosh [1]. However, for N_c, a good agreement was obtained with Manoharan and Dasgupta [7]. On the other hand, the codes of practice underestimate highly these factors and lead to conservative results;
- For an inclined load, the codes of practice largely underestimate the bearing capacity for small load inclinations. However, for great load inclinations, the French code of practice DTU overestimates the bearing capacity of a weightless frictional and cohesive soil. Finally, in the case of a purely cohesive soil, a sliding along the soil-footing interface may occur for small values of the vertical load. The corresponding horizontal stress at the soil-footing interface was found equal to c_u;
- Contrary to the vertical load case where normal and shear stress distributions along the different diameters of the foundation are identical, there is a progressive evolution of these stresses from a diameter to the next one in the inclined load case. Along a given diameter, the normal stress distribution at the soil footing interface is quasi-uniform for the clay and the weightless frictional and cohesive soils and it decreases to zero at the edges for the sand. Concerning the shear stress distribution, both positive and negative shear stresses are observed for large vertical loads. However, for small vertical loads, shear stresses become essentially negative in order to counter weight the horizontal external load.

REFERENCES

1. Kumar, J. and Ghosh, P. (2005). Determination of Nγ for rough circular footing using the method of characteristics, *EJGE*.
2. Bolton, M.D., and Lau, C.K. (1993). Vertical bearing capacity factors for circular and strip footings on Mohr-Coulomb soil. *Can. Geotech. J.*, Vol. 30, 1024–33.
3. Salençon, J., and Matar, M. (1982). Capacité portante des fondations superficielles circulaires. *Journal de Mécanique Théorique et Appliquée*, Vol. 1, N° 2, 237–67.
4. Erickson, H.L., and Drescher, A. (2002). Bearing capacity of circular footings. *J. of Geotech. and Geoenv. Engrg., ASCE*, Vol. 128, N° 1, 38–43.
5. Cassidy, M.J., and Houlsby, G.T. (2002). Vertical bearing capacity factors for conical footings on sand. *Géotechnique*, Vol. 52, N° 9, 687–92.
6. Martin, C.M. (2004). *User guide for ABC - Analysis of Bearing Capacity*. Report No. OUEL 2261/03, Department of Engineering Science, University of Oxford.
7. Manoharan N., Dasgupta S.P. (1995). Bearing capacity of surface footings by finite elements. *Computers & Structures*, Vol. 54, N° 4, 563–586.